Wedge nanostructures for plasmonic nanofocusing

D. Garoli,[1,2,3*] P. Zilio,[1,2] M. Natali,[4] M. Carli,[1,2] F. Enrichi,[5] and F. Romanato[1,2,3]

[1]*Department of Physics "G. Galilei," University of Padova, via Marzolo 8, 35131 Padova, Italy*
[2]*LaNN Laboratory for Nanofabrication of Nanodevices, VenetoNanotech, Corso Stati Uniti 4, 35127 Padova, Italy*
[3]*Institute for Materials Manufacturing (IOM-CNR), Area-Science Park, Basovizza 34012, Trieste, Italy*
[4]*Institute for Inorganic and Surface Chemestry (CNR-ICIS), Corso Stati Uniti 4, 35127Padova, Italy*
[5]*Coord. Interuniversitario Veneto per le Nanotecnologie (CIVEN), via delle Industrie 5, 30175 Marghera (Ve), Italy*
**denis.garoli@venetonanotech.it*

Abstract: We report numerical and experimental results on the optical response of transparent metal coated wedges arrays for plasmonic nanofocusing. Light normally impinging from the dielectric side is coupled to Surface Plasmon Polaritons (SPPs) at the oblique metal-air interfaces. A dielectric phase shifter has been implemented in the structure in order to allow constructive interference of SPPs at the wedge apex. Finite Elements simulations were used to design the system. Focused Ion Beam (FIB) milling, chemical etching and replica molding were used for the fabrication. NSOM and Raman measurements demonstrate that plasmonic nanofocusing actually takes place in the structure.

OCIS codes: (240.6680) Surface plasmons; (220.4241) Nanostructure fabrication; (250.5403) Plasmonics.

References and links

1. D. K. Gramotnev and S. I. Bozhevolnyi, "Plasmonics beyond the diffraction limit," Nat. Photonics **4**(2), 83–91 (2010).
2. A. V. Kabashin, P. Evans, S. Pastkovsky, W. Hendren, G. A. Wurtz, R. Atkinson, R. Pollard, V. A. Podolskiy, and A. V. Zayats, "Plasmonic nanorod metamaterials for biosensing," Nat. Mater. **8**(11), 867–871 (2009).
3. G. Schider, J. R. Krenn, A. Hohenau, H. Ditlbacher, A. Leitner, F. R. Aussenegg, W. L. Schaich, I. Puscasu, B. Monacelli, and G. Boreman, "Plasmon dispersion relation of Au and Ag nanowires," Phys. Rev. B **68**(15), 155427 (2003).
4. E. Verhagen, M. Spasenović, A. Polman, and L. K. Kuipers, "Nanowire Plasmon Excitation by Adiabatic Mode Transformation," Phys. Rev. Lett. **102**(20), 203904 (2009).
5. K. Kato, A. Ono, W. Inami, and Y. Kawata, "Plasmonic nanofocusing using a metal-coated axicon prism," Opt. Express **18**(13), 13580–13585 (2010).
6. N. C. Lindquist, P. Nagpal, A. Lesuffleur, D. J. Norris, and S.-H. Oh, "Three-Dimensional Plasmonic Nanofocusing," Nano Lett. **10**(4), 1369–1373 (2010).
7. P. Nagpal, N. C. Lindquist, S.-H. Oh, and D. J. Norris, "Ultrasmooth Patterned Metals for Plasmonics and Metamaterials," Science **325**(5940), 594–597 (2009).
8. M. Ohtsu, K. Kobayashi, T. Kawazoe, S. Sangu, and T. Yatsui, "Nanophotonics: design, fabrication, and operation of nanometric devices using optical near fields," IEEE J. Sel. Top. Quantum Electron. **8**(4), 839–862 (2002).
9. D. K. Gramotnev and K. C. Vernon, "Adiabatic nano-focusing of plasmons by sharp metallic wedges," Appl. Phys. B **86**(1), 7–17 (2006).
10. M. I. Stockman, "Nanofocusing of Optical Energy in Tapered Plasmonic Waveguides," Phys. Rev. Lett. **93**(13), 137404 (2004).
11. M. W. Vogel and D. K. Gramotnev, "Shape effects in tapered metal rods during adiabatic nanofocusing of plasmons," J. Appl. Phys. **107**(4), 044303–044311 (2010).
12. D. K. Gramotnev, M. W. Vogel, and M. I. Stockman, "Optimized nonadiabatic nanofocusing of plasmons by tapered metal rods," J. Appl. Phys. **104**(3), 034311–034319 (2008).
13. D. F. P. Pile, T. Ogawa, D. K. Gramotnev, T. Okamoto, M. Haraguchi, M. Fukui, and S. Matsuo, "Theoretical and experimental investigation of strongly localized plasmons on triangular metal wedges for subwavelength waveguiding," Appl. Phys. Lett. **87**(6), 061106 (2005).

#167642 - $15.00 USD Received 30 Apr 2012; revised 25 May 2012; accepted 2 Jun 2012; published 2 Jul 2012

14. A. Boltasseva, V. S. Volkov, R. B. Nielsen, E. Moreno, S. G. Rodrigo, and S. I. Bozhevolnyi, "Triangular metal wedges for subwavelength plasmon-polariton guiding at telecom wavelengths," Opt. Express **16**(8), 5252–5260 (2008).
15. F. De Angelis, R. P. Zaccaria, M. Francardi, C. Liberale, and E. Di Fabrizio, "Multi-scheme approach for efficient surface plasmon polariton generation in metallic conical tips on AFM-based cantilevers," Opt. Express **19**(22), 22268–22279 (2011).
16. D. O'Connor, M. McCurry, B. Lafferty, and A. V. Zayats, "Plasmonic waveguide as an efficient transducer for high-density data storage," Appl. Phys. Lett. **95**(17), 171112 (2009).
17. K. C. Vernon, D. K. Gramotnev, and D. F. Pile, "Adiabatic nanofocusing of plasmons by a sharp metal wedge on a dielectric substrate," J. Appl. Phys. **101**(10), 104312 (2007).
18. E. Verhagen, L. K. Kuipers, and A. Polman, "Plasmonic nanofocusing in a dielectric wedge," Nano Lett. **10**(9), 3665–3669 (2010).
19. H. Raether, *Surface Plasmons* (Springer-Verlag, 1988).
20. D. K. Gramotnev, "Adiabatic nanofocusing of plasmons by sharp metallic grooves: Geometrical optics approach," J. Appl. Phys. **98**(10), 104302 (2005).
21. D. F. P. Pile and D. K. Gramotnev, "Adiabatic and nonadiabatic nanofocusing of plasmons by tapered gap plasmon waveguides," Appl. Phys. Lett. **89**(4), 041111 (2006).
22. E. Moreno, S. G. Rodrigo, S. I. Bozhevolnyi, L. Martín-Moreno, and F. J. García-Vidal, "Guiding and Focusing of Electromagnetic Fields with Wedge Plasmon Polaritons," Phys. Rev. Lett. **100**(2), 023901 (2008).
23. W. Chen, D. C. Abeysinghe, R. L. Nelson, and Q. Zhan, "Experimental confirmation of miniature spiral plasmonic lens as a circular polarization analyzer," Nano Lett. **10**(6), 2075–2079 (2010).
24. S. Yamamoto and H. Watarai, "Surface-Enhanced Raman Spectroscopy of Dodecanethiol-Bound Silver Nanoparticles at the Liquid/Liquid Interface," Langmuir **22**(15), 6562–6569 (2006).

1. Introduction

In recent years there was an increasing interest in theoretical, numerical, and experimental investigations of strongly localized surface plasmons in patterned metallic nanostructures [1]. In fact, a properly designed structure offers unique opportunities for making integrated optics devices with subwavelength localization of light [1]. An effective concentration of electromagnetic energy at nano-scale region can be obtained by several metal structures such as nanorods [2], nanostrips [3,4], dielectric conical tips coated by a metal film [5], nanopyramids [6,7] and metallic nanowedge [7–9]. These structures can find important applications in all the fields where nano-scale resolution is essential, such as near field optical microscopy, electromagnetic probing of separate molecules and quantum dots, non-linear plasmonics, etc.

The study of plasmonic subwavelength localization has introduced the concept of *nanofocusing* [10], i.e. the concentration of light into regions with dimensions significantly smaller than those allowed by the diffraction limit of light. It has been theoretically demonstrated [10] that Surface Plasmon Polaritons (SPPs) propagating toward the tip of a sharp tapered metallic waveguide are slowed down, i.e. their phase and group velocities turn to zero, leading to huge EM field enhancements. This phenomenon, referred to as *adiabatic* nanofocusing, causes accumulation of energy and giant local fields at the tip. The term adiabatic refers to the absence of power losses involved in the phenomenon other than metal dissipation [10,11]. In other words, most of the electromagnetic energy carried by the converging SPP waves is concentrated on the focusing site, while a fraction is lost in metal heating. This strictly happens only in presence of very sharp tips and wedges (apertures angles narrower than few degrees). In presence of larger aperture angles still a nanofocusing effect takes place, although weakened by SPP back reflections from the tip and radiative losses [12]. This case is commonly referred to as *non-adiabatic* nanofocusing.

Among the different possible structures, we are interested in plasmonic field localization at the edge of a metal-coated dielectric wedge. Gramotnev and Vernon [9], in fact, demonstrated that nanofocusing takes place when SPPs propagate along the sides of a sharp metallic wedge toward the ridge. This has been recently studied by several authors [7, 13, 14].

As pointed out in the aforementioned work [9], one major issue in order to obtain the nanofocusing effect is proper excitation of the SPPs converging towards the tip. Sharp metal wedges show nanofocusing effects only when an even thin-film plasmonic mode is excited

#167642 - $15.00 USD Received 30 Apr 2012; revised 25 May 2012; accepted 2 Jun 2012; published 2 Jul 2012

(i.e. electric field is symmetric with respect to the plane of symmetry of the structure) [9]. In this paper, we present an innovative optical design enabling both efficient coupling of light to SPPs and the correct in-phase matching of SPPs at the wedge edge. It consists in the combination of transparent metal-coated wedges, which allow SPP coupling due to refractive index contrast, with a dielectric step-like phase shifter. The overall plasmonic mode which is obtained close to the edge mimics the TM mode associated to the adiabatic compression of plasmons in a tapered metal nanowedge. Although the generation of TM modes from far field to near field in plasmonic tapered structures was already investigated [4, 5, 15], to the best of our knowledge no experimental verification of the nanofocusing effect has been provided using the optical layout we propose.

Full field Finite Elements simulations allowed verifying the effectiveness of the design. Moreover it will be shown that, optimizing materials and geometrical parameters, a valuable field enhancement at the wedge edge can be obtained with this kind of focusing structure. This enhancement, although not comparable to that obtained with 3D focusing structures, demonstrates that the proposed scheme for coupling and phase matching can be effectively exploited for nanofocusing purposes.

Beside efficient plasmonic modes excitation, other extremely important issues in realizing effective nanofocusing structures are metal surface quality and tip sharpness of the fabricated nanostructures. In fact, as previously reported [7], surface plasmons are very sensitive to surface inhomogeneities, which can cause enhanced metal losses, scattering, and limited propagation. The choice of a fabrication process ensuring very sharp features, in particular very low tips radii, is therefore of fundamental importance in order to achieve large field enhancements [11,16]. A fabrication strategy leading to very smooth surfaces and sharp edges has been proposed and used by Napgal et al. [7] and Boltasseva et al. [14]. In these papers the template stripping process not only allows to replicate wedge shaped structures with high surface and edge quality, but it also results in a very efficient process to prepare many other metallic nanostructures. Taking advantage of these ideas, we report a fabrication process that by means of a single replica realizes the desired optical design of sharp metal-coated dielectric wedge. Template stripping based on replica in transparent polymer, coupled with metal evaporation, allowed us to obtain few nanometers curvature radii at the wedge ridge. The transparency of the substrate enables illumination of the wedge from the high-refractive index dielectric side and therefore effective coupling to SPP modes. The proposed layout is much simpler to obtain than axially symmetric configurations proposed in literature. These structures theoretically provide higher field enhancements (up to factors 1000), but their performance crucially depends on the curvature radius at the tip [11,16], which is very difficult to control in fabrication.

The experimental verification of the nanofocusing effects in the fabricated device layout is obtained by means of both Near-field Scanning Optical Microscopy (NSOM) and Raman spectroscopy measurements. The resulting near-field intensity images are interpreted by means of FEM optical simulations, and provide evidence that the focusing effect actually takes place.

2. Device layouts and simulations

A number of experimental setups may be adopted in order to verify the nanofocusing properties of wedge plasmonic structures [8,17,18]. In this paper we present a device setup which resembles the well-known Kretschman-Raether [5,19] SPPs generation scheme. We consider first the layout sketched in Fig. 1(a). Transparent dielectric wedges are coated with a thin metallic film. Air is supposed to be present in the other half-space. TM polarized light with proper frequency impinges normally onto the plane of the wedge from the transparent dielectric side. This may excite thin-film plasmons polaritons on the metal-air interfaces of the film on the wedges, in a similar way as in the Kretschmann-Raether SPP coupling scheme. The electric fields of the SPPs generated on each side of the wedge in this

#167642 - $15.00 USD Received 30 Apr 2012; revised 25 May 2012; accepted 2 Jun 2012; published 2 Jul 2012

configuration are π-out-of-phase and are thus expected to undergo disruptive interference when they reach the wedge tip.

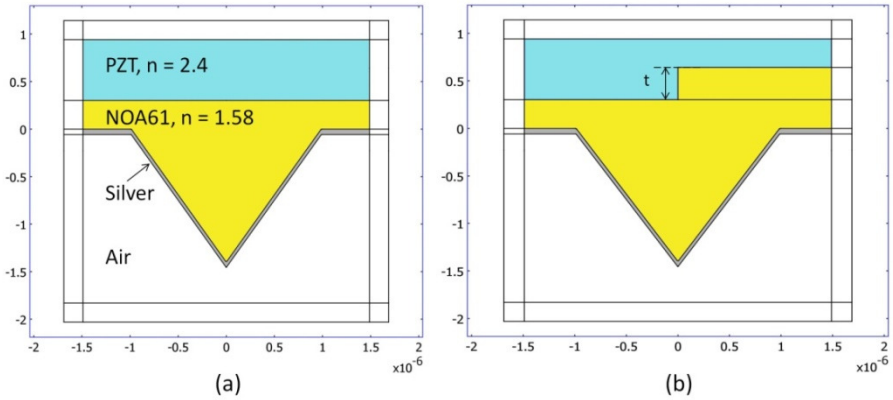

Fig. 1. Devices layouts of the simulated metal coated dielectric nanowedge structures. Configuration without (a) and with (b) phase shifter. TM polarized plane waves impinges normally onto the structures from the top Wedge aperture is 70.4° as reported in the text.

In order to obtain in-phase SPPs at the wedge edge, the condition of illumination must be changed. The wedge, in fact, must be illuminated with π-out-of-phase light on one side with respect to the other side. This can be obtained with the setup shown in Fig. 1(b). Immediately before the metal coated wedge, a step-like dielectric phase shifter is introduced, whose height, *t*, is given by

$$\frac{2\pi}{\lambda} t \left| n_1 - n_2 \right| = \pi \qquad (1)$$

being λ the impinging wave vacuum wavelength, n_1 and $n_2$are the refractive indexes of the lower and upper media, respectively. With this configuration SPPs generated on each side of the wedge approach the edge in phase and are thus expected to constructively interfere. As reported by several authors [10,20,21], the field enhancement expected in this case is much higher than that obtained by the trivial sum of two SPP waves, because of the nanofocusing effect.

In order to verify the plasmonic effects outlined above and to properly design the structure to maximize the field enhancement at the tip, we simulated the full electromagnetic fields by means of COMSOL Multiphysics commercial software which implements the Finite Elements Method (FEM). The FEM models layouts are reported in Fig. 1(a) and 1(b).Since the structure is inherently invariant along the out-of-plane dimension, 2D simulations were performed. A port excitation is set at the upper boundary, providing a unit power of incident light. Perfectly Matched Layers are placed all around the model in order to properly absorb light scattered from the structure. Model discretization is performed by means of the COMSOL automatic meshing tool. In particular, different mesh sizes were used in different parts of the model in order to maximize resolution in the regions of steepest variations of the fields, keeping at the same time reasonable the computational costs. Triangular mesh elements were used with maximum element sizes of 20nm in the dielectric regions far from the wedge edge. Since high field gradients are expected at the wedge edge we set here a progressively finer mesh, down to 0.5 nm minimum element size. This mesh resolution turned out to be sufficient both to resolve the field gradients and to provide a fully converged solution.

The first issue we dealt with in designing the structure was finding the optimal combination of materials, metal thickness and incident wave vacuum wavelength in order to

#167642 - $15.00 USD Received 30 Apr 2012; revised 25 May 2012; accepted 2 Jun 2012; published 2 Jul 2012

maximize the SPP coupling for a given wedge aperture. As will be discussed in the next section, wedge aperture is fixed to 70.4° by the chosen fabrication technique. This aperture angle limits the efficiency achievable with this structure [22], but leads to important smoothness in the final fabricated samples. The dielectric material constituting the wedge is also fixed by experimental issues (NOA61), having a refractive index of ~1.58 at visible wavelengths. The upper material was then chosen to have a much higher refractive index, in order to obtain the desired phase shift within relatively small thicknesses, according to Eq. (1). Lead ZirconateTitanate (PZT) was chosen, having a refractive index of ~2.4 in the spectral range of interest. For the metal coating, gold and silver were considered.

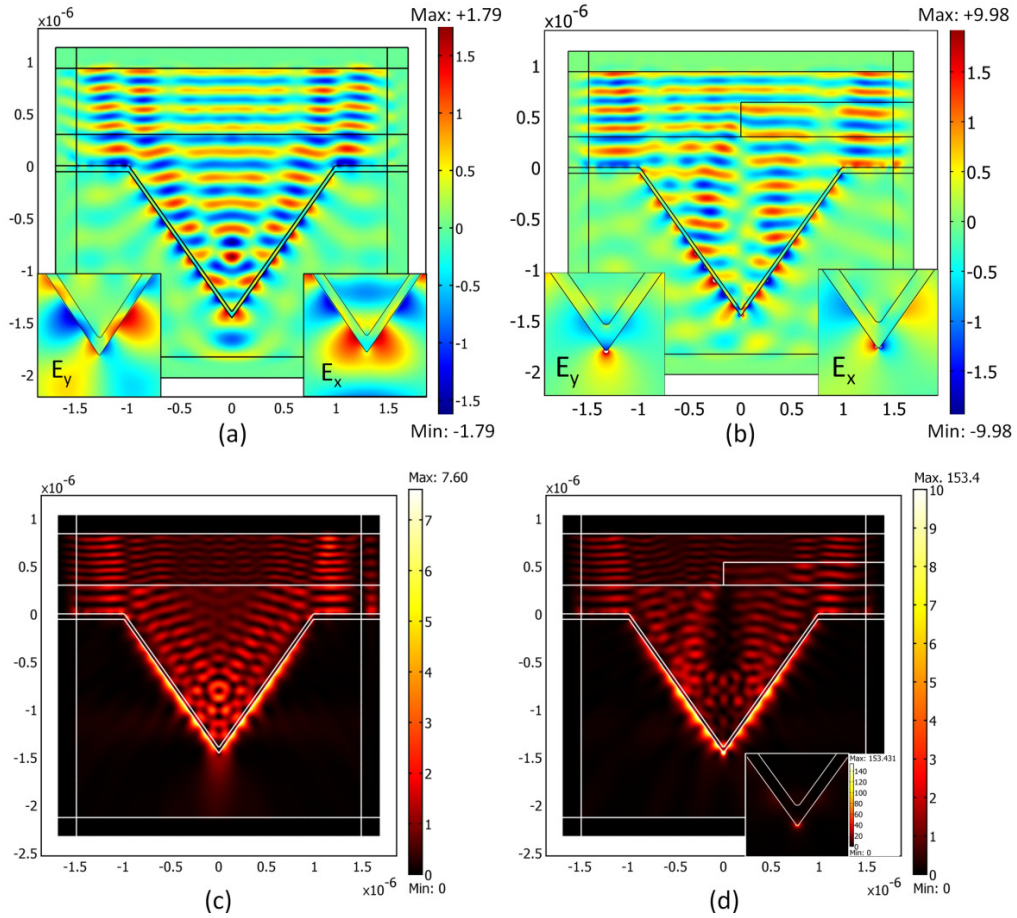

Fig. 2. (a), (b) Full field simulated x component in the presence and absence of the phase shifter. Insets: zooms on the wedges edge; (c), (d) Field intensity maps. The fields are normalized to the amplitude of the impinging wave in vacuum. Note that in (d) the maximum field value is well above the maximum color scale value. Geometrical parameters of the structure are the following: wedge height: 1.4μm, metal thickness on the wedge sides: 33nm, phase shifter thickness: 238.6nm, curvature radius at the wedge edge: 5nm. TM polarized light with vacuum wavelength λ = 390nm impinges normally on the structures from above.

We thus investigated SPP coupling efficiencies of TM-polarized monochromatic plane waves, impinging at an angle of 54.8° onto different PZT-NOA61-metal-air interfaces. It has been demonstrated [21] that the curvature radius at the wedge edge crucially influences the extent of EM field focusing. As will be discussed in next section, the adopted nanofabrication technique allows obtaining a very small curvature radius, which in our case is about 5nm. For

#167642 - $15.00 USD Received 30 Apr 2012; revised 25 May 2012; accepted 2 Jun 2012; published 2 Jul 2012

this reason, the tip curvature radius was kept fixed as a result of the constraints imposed by the fabrication process. On the contrary, wedge dimensions, metal coating material and thickness and illumination wavelength have been set as varying parameters in order to maximize field enhancement at the wedge edge. High efficiencies were found in the UV part of the spectrum, while proper metal thicknesses were found to be around 30 nm.

In Fig. 2 we report the simulation results of the optimal layout in absence (Fig. 2(a) and 2(c)) and presence (Fig. 2(b) and 2(d)) of phase shifter. Optimum geometrical and physical parameter values are reported in the figure caption. Silver turned out to give the best performance due to its lower dissipation rate at UV-VIS wavelengths. Surface plasmon dynamics is well visualized looking at the components of the Electric field in the two configurations, with and without the phase shifter, respectively Fig. 2(a) and 2(b). As can be seen, light coupling to SPP modes takes place at both sides of the NOA61-silver interface, with low reflections. In absence of the phase shifter, SPPs reaching the wedge edge have opposite E_y fields and parallel E_x fields. SPPs destructively interfere at the tip and power is therefore coupled to propagating waves in the air domain. On the other hand, in the presence of the phase shifter, SPPs constructively interfere in a very small metal region very close to the edge (see Fig. 2(b), insets). As can be seen in Fig. 2(d) a remarkably high intensity enhancement at the wedge edge is predicted in the latter case, with a maximum enhancement factor around 150 (note that the maximum intensity value lies well outside the color scale range, see also the inset plot). On the contrary, no enhancement at the wedge's tip is found in absence of phase shifter, as expected.

3. Fabrication

The fabrication of wedges array requires few steps of process: Focused Ion Beam (FIB) lithography; wet etching; material evaporation and replica molding. A SiO_2 layer of approximately 500nm has been thermally grown on Si <100> in a hot furnace. This oxide layer has been patterned by FIB lithography by means of a FEI nova 600i dual beam. An array of rectangles (500nm deep, 3μm wide) over an area of 640μmx640μm has been fabricated with a single exposure. After the exposure, an anisotropic KOH wet etching has been performed to obtain V-grooves defined by crystalline Si (111) atomic planes thus obtaining the negative of the desired structure. The KOH etching along the (111) planes fixes the wedge aperture angle at 70.4°. As reported above, the optimal configuration comprises 33nm of silver deposited onto the wedge. With these parameters, the best focusing performance occurs at a wavelength of 390nm. Unfortunately, we are not equipped for near-field optical characterizations at this wavelength. Nevertheless, the experimental verification of the nanofocusing effect can be carried out also at higher wavelengths, even if a lower intensity enhancement is expected. We therefore used a standard 514 nm laser light. This is easily available by common argon gas lasers which can be fiber-coupled to our microscopic systems. Moreover, gold was used instead of silver, since at 514nm it turned out to provide better coupling and it is not affected by oxidation. The intensity enhancement expected in our case is a factor 7.4. In order to decrease the adhesion of Au on Si, the patterned grooves were previously oxidized in air for 5 hours at 1000°C. Hence, the e-beam evaporation of 33nm Au was performed on the SiO_2 layer. The metallized grooves array was then used as a master for replication into NOA61 (transparent thiolene optical adhesive from Norland Optical Adhesives) by UV curing to obtain negative copies, i.e. wedges.

As illustrated above, a digital grating placed at the bottom of the wedge ensures the required π phase shift between the two halves of the wedge (see Eq. (1)). The phase shifter has been realized by mean of FIB lithography on a ITO/glass substrate where a commercial PZT52/48 sol-gel solution (Inostek) layer with n = 2.4 (@514nm) was previously spin coated at 3600 rpm and annealed at 300°C for 30 min. After repeating the spin-coating and baking process 4 times the samples are annealed in a muffle furnace at 450°C yielding a PZT film thickness of ca. 400 nm. The NOA61 refractive index can be taken to be 1.58 in the VIS

#167642 - $15.00 USD Received 30 Apr 2012; revised 25 May 2012; accepted 2 Jun 2012; published 2 Jul 2012

spectrum. Therefore the correct thickness of the phase shifter turns out to be 313nm. Integration of FIB patterned phase shifter grating with the grooves pattern was obtained by pressing a drop of NOA61 between the metallized Si master and the phase-shifter substrate, then aligning the two patterns under an optical microscope and compressing the stack in a manual hydraulic press at ca. 100 bar. After 10 minutes of compression UV curing is performed by illuminating the sample - still under pressure - through a transparent thick glass plate that acts as a top compression plate. The compression process is necessary to maintain a small (< 500 nm) distance between the wedge base and the phase shifter pattern. UV curing was performed using a 100 Watt UV flood lamp (SB100P spectroline) optimized for 365 nm wavelength. With the NOA replica a stripping effect removes Au from the oxidized Si mold and covers the NOA wedges. This process allows to obtain wedge tip with radius of curvature below 5nm.In Fig. 3 optical (a) and SEM (b) images of the prepared wedges array are reported. In particular, the inset in Fig. 3(b) reports details of the obtained tip radius. It is worth to notice that the phase shifter patterns were intentionally rotated by ca. 25 degrees with respect to the wedge array direction before compression, so that the correct conditions for phase shifting exist only at the points where the wedge edges cross the phase shifter stripes (Fig. 3(a)).This approach allows to compare the behavior of the structure in optimal and non-optimal configuration. The correct in-phase condition, in fact, is obtained only at discrete points along the wedge, while elsewhere the effect is expected to be zero or modulated by the incorrect phase shifter position.

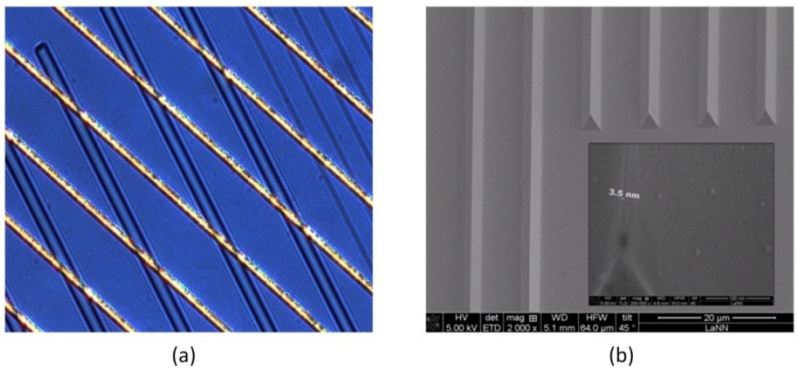

(a) (b)

Fig. 3. (a) Optical Microscope image of a prepared sample (b) SEM micrographs of the replicated nanowedge sample. (the inset reports a detail of the wedge's tip).

4. Optical characterizations

4.1.Near-field Scanning Optical Microscopy (NSOM)

Experimental near-field analysis has been performed by means of NSOM using a confocal Witec microscope equipped with a fiber-coupled 150 mWAr^+ laser with a wavelength of 514 nm. The sample is illuminated from the back of the wedge structure with TM-polarized light. An aperture metal-coated NSOM tip was used to collect the spatial intensity profile of the near-field surrounding the wedges. Figure 4 reports a NSOM map of light intensity over an area 50µm x50µm, showing the details on five wedges of the array. An intensity peak is observed at the wedges tip and a minimum of the intensity is present in correspondence with the phase shifter.

#167642 - $15.00 USD Received 30 Apr 2012; revised 25 May 2012; accepted 2 Jun 2012; published 2 Jul 2012

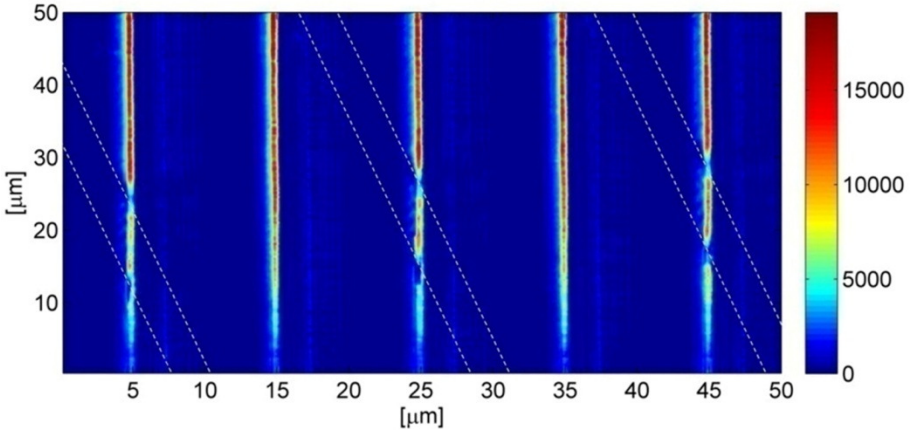

Fig. 4. NSOM maps of the prepared sample comprising the digital grating phase shifter (highlighted by the dashed lines). TM polarized 514nm light was used. The darker spots correspond to the intersection between the wedges and the grating below.

In order to better understand the experimental results, a FEM simulation of the interaction between the NSOM tip and the wedge structure has been performed (Fig. 5).A schematic NSOM tip was included in the simulation domain, beside the full wedge and phase shifter layout. The NSOM tip was modeled as an Al coated hollow pyramid with a 100nm-sized central hole. All geometrical parameters of the wedge focusing structure were set to match the ones of the fabricated sample, in order to faithfully reproduce the results of the experimental characterization. Experimental gold dielectric constants were used (obtained from ellipsometric measurements). We calculated the fraction of light power transmitted from the tip into the hollow pyramid, which models the NSOM intensity signal sensed by the detector. In Fig. 5 we report the out-of-plane magnetic field H_z for configurations with and without phase shifter. As can be seen directly from these field maps, no signal is transmitted when the phase shifter is present (Fig. 5(a)), while a non-zero signal is transmitted in its absence (Fig. 5(b)).In order to simulate a NSOM scan of the wedge edge the calculation was repeated for several y positions of the phase shifter with respect to the wedge symmetry axis. In particular the initial and final phase shifter positions are set sufficiently far from the wedge edge y position in order to reproduce the optical configuration of Fig. 1(a) in which no phase shifter is seen above the wedge structure.

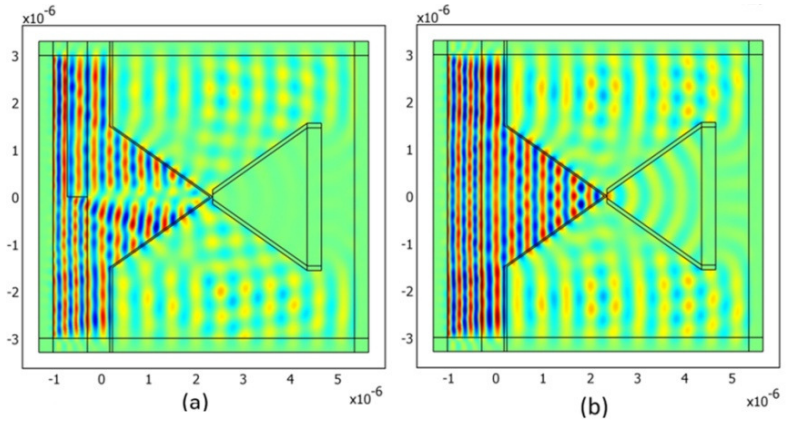

Fig. 5. Simulated transverse magnetic field (H_z) distribution in the presence of a NSOM probe.(a) Configuration with the phase shifter; (b) Configuration without the phase shifter. The geometrical parameters of the simulations match the ones of the best sample fabricated.

#167642 - $15.00 USD Received 30 Apr 2012; revised 25 May 2012; accepted 2 Jun 2012; published 2 Jul 2012

The calculated power transmitted into the hollow pyramid as a function of the position of the phase shifter is reported in Fig. 6(a) (green line), taking into account the 25° angle between wedges and phase shifter. A minimum NSOM intensity signal is predicted in presence of nanofocusing at the wedge edge.

This is somewhat counterintuitive since it can be expected the NSOM signal to be sensitive to the near-field intensity and therefore being maximum in presence of strong nanofocusing at the wedge edge. However it is well known that the NSOM probe often perturbs the near field distributions and the NSOM intensity map is the result of sample-probe interactions which are strongly correlated to sample morphology. Moreover, this result is confirmed by data reported in literature for apertured-tip NSOM measurements [23].In Fig. 6(a) we also report the experimental near field intensity measured along a wedge edge (blue line). As can be seen the measured intensity when the NSOM probe passes over a crossing between a wedge and the underlying phase shifter exhibits a dip, whose width is in good agreement with the simulation. From this data we can infer that the nanofocusing effect actually takes place at the wedge-phase shifter crossing, manifesting itself as a minimum of NSOM signal in correspondence of these points. For comparison we report in Fig. 6(b) the result of the same simulation performed with the optimal device layout described in section 2 (Silver-coated wedge, 1.4μm high, see caption of Fig. 2).

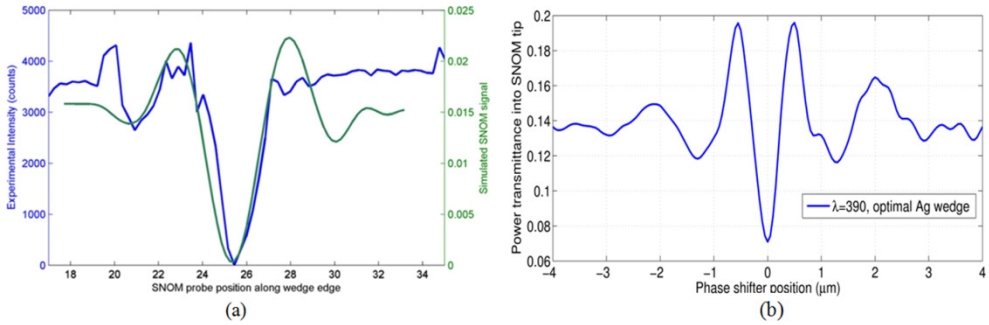

Fig. 6. (a) Comparison between experimental (blue) and simulated (green) NSOM signal along a wedge ridge. (b) Simulated NSOM signal along a wedge ridge at 390nm for the optimized structure.

4.2. Raman spectroscopy

In order to verify the field enhancement at the wedge's tip, experimental analyses based on Raman/SERS (Surface Enhanced Raman Spectroscopy) spectroscopy have been performed. Exploiting the fact that the SERS signal is local, proportional to $|E|^4$, and roughly independent of the field direction, we expect an enhanced signal in correspondence of the intersection between the wedge ridge and the digital grating below.

A wedge array sample has been functionalized with a self-assembled monolayer of dodecanethiol ($C_{12}H_{25}SH$) deposited on the gold surfaces at room temperature. Samples were pre-cleaned in a basic peroxide solution (5:1:1 double distilled H2O, 30% H_2O_2 and 25% NH_4OH) for 10 minutes, rinsed in double distilled water and dried under N_2 flux. The cleaned samples were immersed in a 4-mM solution of dodecanethiol in ethanol for about 48 hrs. and therefore rinsed thoroughly with ethanol for at least 5 minutes, followed by drying under nitrogen stream. The spontaneous assembly of the molecules is known to form a densely packed and highly oriented structure on a metallic surface. The SERS spectrum from the functionalized sample was then measured by means of a confocal micro-Raman Witec instrument. The system is equipped with a 150 mWAr^+ laser, fiber coupled to the optical microscope and focused on the sample surface by a 100x objective. The emitted signal is analyzed by a single grating spectrometer coupled to an Andor DU401 CCD detector,

#167642 - $15.00 USD Received 30 Apr 2012; revised 25 May 2012; accepted 2 Jun 2012; published 2 Jul 2012

enabling the acquisition of local micro-Raman spectra. The spatial resolution is about 0.5 x 0.5 µm laterally and 1 µm in depth. SERS maps can be obtained by integrating the Raman peak signal for each point of a defined grid.

A map along a wedge ridge was collected integrating the Raman peak of dodecanethiolat 707cm^{-1} (υ (C-S) [24]). Figure 7(a) compares the acquired spectra of a functionalized (solid blue line) and a bare (dashed red line) sample. Figure 7(b) reports the result of this measurement showing the intersection between the wedge and the phase shifter.

As can be seen, two maxima are found as expected in correspondence of the crossing between wedge and underlying phase shifter. Actually, as can be seen, the measured Raman enhancement factor at the phase shifter-wedge crossings is rather small, around a factor 25. This reflects the non-ideality of the fabricated structure and is mainly due to the high losses in the gold layer. Nevertheless, the Raman measurement provides direct evidence of the nanofocusing phenomenon.

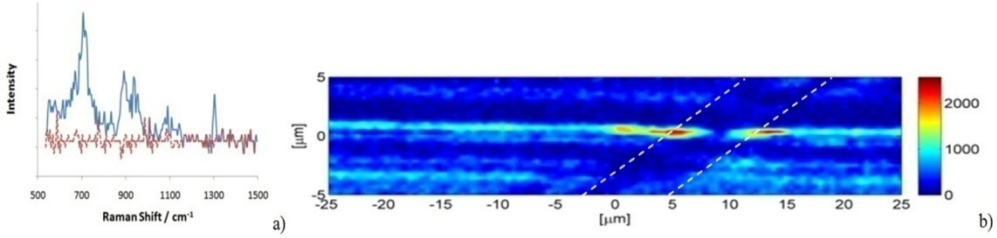

Fig. 7. (a) Comparison between the Raman spectra obtained from a functionalized (solid blue line) and a bare sample (dashed red line). (b) Raman map of a wedge. The intersection between the wedge and the digital phase shifter is highlighted and two maximum of intensity are observed in correspondence of the intersection.

4. Conclusions

A valuable nanofocusing effect takes place in a metal coated wedge configuration, provided that the correct phase shift illumination conditions are set and geometrical parameters are optimized. Gold coated NOA wedge arrays were fabricated by means of FIB and wet etching obtaining good control of the wedge size and radius of the tip of about 5nm. The correct phase modulation at the wedge profile was achieved with a single step of imprinting. Finite Elements simulations of metal coated wedges were carried out showing that these structures can effectively focus light at the nanoscale. The plasmonic nanofocusing effect was demonstrated by means of NSOM and Raman (SERS) measurements showing the strong potentialities of this system for nano-optics purposes

Acknowledgments

This work has been supported by a grant from "FondazioneCariparo" - Surface PLasmonics for Enhanced Nano Detectors and Innovative Devices (SPLENDID) – Progetto Eccellenza 2008 and from University of Padova – Progetto di Eccellenza "PLATFORM". Support has also been provided by the Doctoral School in Materials Science and Engineering of Padova University.

#167642 - $15.00 USD Received 30 Apr 2012; revised 25 May 2012; accepted 2 Jun 2012; published 2 Jul 2012